PAPER

Enhanced chemical looping CO_2 conversion activity and thermal stability of perovskite $LaCo_{1-x}Al_xO_3$ by Al substitution†

Yoshihiro Goto, [ID] * Kiyoshi Yamazaki,* Masashi Kikugawa and Masakazu Aoki

The reverse water–gas shift chemical looping (RWGS-CL) process that utilizes redox reactions of metal oxides is promising for converting CO_2 to CO at low temperatures. Metal oxides with perovskite structures, particularly, perovskite $LaCoO_3$ are promising frameworks for designing RWGS-CL materials as they can often release oxygen atoms topotactically to form oxygen vacancies. In this study, solid solutions of perovskite $LaCo_{1-x}Al_xO_3$ ($0 \leq x \leq 1$), which exhibited high CO production capability and thermal stability under the RWGS-CL process, were developed. Al-substituted $LaCo_{0.5}Al_{0.5}O_3$ ($x = 0.5$) exhibited a 4.1 times higher CO production rate (2.97×10^{-4} CO mol g^{-1} min^{-1}) than that of $LaCoO_3$ ($x = 0$; 0.73×10^{-4} CO mol g^{-1} min^{-1}). Diffuse reflectance infrared Fourier transform spectroscopy studies suggested that an increase in CO_2 adsorption sites produced by the coexistence of Al and Co was responsible for the enhancement of CO production rate. Furthermore, $LaCo_{0.5}Al_{0.5}O_3$ maintained its perovskite structure during the RWGS-CL process at 500 °C without significant decomposition, whereas $LaCoO_3$ decomposed into La_2O_3 and Co^0. In situ X-ray diffraction study revealed that the high thermal stability was attributed to the suppression of phase transition into a brownmillerite structure with ordered oxygen vacancies. These findings provide a critical design approach for the industrial application of perovskite oxides in the RWGS-CL processes.

Introduction

The development of technologies to convert carbon dioxide (CO_2) into valuable compounds is essential for mitigating anthropogenic global warming and meeting the growing demand for energy and chemical products. The global CO_2 emissions have increased annually, reaching an all-time high in 2022 (36.8 Gt per year from energy combustion and industrial process).[1] Carbon capture and storage technologies[2–4] are being actively investigated to reduce the CO_2 emissions; however, currently, the annual amount of storage capacity (243.97 Mt in 2022)[5] is only 0.66% of the global CO_2 emissions, resulting in most of the emissions being released into the atmosphere. Capturing this atmospheric CO_2 using direct air capture technologies[6] and utilizing it can indirectly mitigate the global CO_2 emissions.[7]

A possible first step in utilizing captured CO_2 is to convert it into carbon monoxide (CO), which serves as a crucial raw material for synthetic fuels and various chemical products.[8] This conversion is generally carried out by a catalytic reverse water–gas shift reaction (RWGS reaction; $CO_2 + H_2 \rightarrow CO + H_2O$), which requires high temperature due to thermodynamic constraints.[9] For example, temperatures greater than 750 °C are required to achieve a CO_2 conversion of 80%. To decrease this operating temperature, the RWGS chemical looping (RWGS-CL) process using metal oxides has been actively investigated in recent years.[10] The RWGS-CL process consists of sequential reactions of reduction ($MO_x + \delta H_2 \rightarrow MO_{x-\delta} + \delta H_2O$) and re-oxidation ($MO_{x-\delta} + \delta CO_2 \rightarrow MO_x + \delta CO$) of metal oxides. In contrast to catalytic RWGS reaction, which uses a mixture of H_2 and CO_2 in a certain ratio, the RWGS-CL process is not limited by thermodynamic constraints because the reduction and the oxidation processes are separate, exhibiting the potential for high CO_2 conversion even at low temperatures (<500 °C).[11] Moreover, continuous CO production is achieved by using a fixed bed system in which H_2 and CO_2 are alternately provided to two reactors filled with metal oxides (Fig. 1a) or a circulating fluidized bed system (Fig. 1b) in which the metal oxides are circulated between the oxidation and the reduction reactors.[12]

Toyota Central R&D Labs., Inc., 41-1 Yokomichi, Nagakute, Aichi 480-1192, Japan. E-mail: yoshihiro-goto@mosk.tytlabs.co.jp, e0936@mosk.tytlabs.co.jp
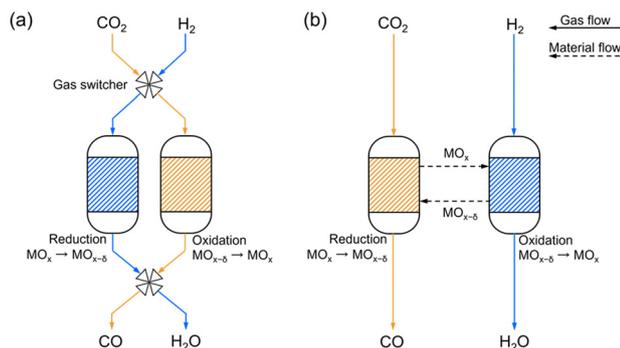
Fig. 1 CO production flowchart based on reverse water−gas shift reaction chemical looping (RWGS-CL) process using (a) periodically operated fixed bed system and (b) circulating fluidized bed system.

These systems do not require a water separation process for the produced CO and do not generate methane as a common by-product, resulting in the RWGS-CL process demonstrating higher energy efficiency than the catalytic RWGS reaction.[13]

The performance of the RWGS-CL process is substantially affected by the metal oxides that are responsible for the reduction and re-oxidation reactions. Metal oxides, where some transition metals (*e.g.*, Mn, Fe, Co, and Ni)[14–17] and some triels (In and Ga)[11,18] act as redox species, have been reported as materials for the RWGS-CL process (RWGS-CL materials). To produce CO in the oxidation process with CO_2, RWGS-CL materials are required to form a large number of oxygen vacancies, which work as active sites for CO_2 conversion, in the reduction process with H_2.[19] Metal oxides with perovskite structures can often release oxygen atoms topotactically to form oxygen vacancies; hence, they are promising frameworks for designing RWGS-CL materials. In particular, perovskite $LaCoO_3$, which demonstrates catalytic RWGS reaction activity,[20] is capable of stabilizing a large number of oxygen vacancies.[21] However, $LaCoO_3$ is not suitable for the RWGS-CL process because of its poor thermal stability in a reducing atmosphere (decomposition starts at 500 °C).[22] We recently demonstrated that the thermal stability of perovskite $LaNiO_3$ can be enhanced by Al substitution of a Ni site.[23] In this study, we attempted Al substitution of a Co site in perovskite $LaCoO_3$ and investigated the effects of Al substitution on thermal stability in a reducing atmosphere and RWGS-CL performance. Al substitution enhanced the thermal stability and prevented phase decomposition at a typical operating temperature of 500 °C during the RWGS-CL process. Notably, although the number of oxygen vacancies formed in $LaCo_{1-x}Al_xO_3$ decreased with increasing Al substitution, the CO production rate increased. $LaCo_{0.5}Al_{0.5}O_3$ did not exhibit any degradation after 32 cycles of the RWGS-CL stability test, indicating that $LaCo_{1-x}Al_xO_3$ has potential as a RWGS-CL material.

Experimental

Polycrystalline $LaCo_{1-x}Al_xO_3$ (x = 0, 0.25, 0.5, 0.75, and 1) solid solution samples were prepared using the polymerized complex method. $La(NO_3)_3 \cdot 6H_2O$ (99.9%, FUJIFILM Wako Chemicals), $Co(NO_3)_2 \cdot 6H_2O$ (99.9%, FUJIFILM Wako Chemicals), $Al(NO_3)_3 \cdot 9H_2O$ (99.997%, Sigma-Aldrich), citric acid (98%, FUJIFILM Wako Chemicals), and ethylene glycol (99%, FUJIFILM Wako Chemicals) were dissolved in a minimum amount of deionized water in a $1 : (1 - x) : x : 6 : 6$ molar ratio. The prepared solutions were stirred on a hotplate at 90 °C for 30 min to promote polymerization and at 150 °C until the brown gels dried. The obtained gels were preheated at 400 °C for 2 h and then calcined twice at 800 °C for 5 h in air. $La_{0.6}Ca_{0.4}Fe_{0.4}Mn_{0.6}O_3$ and Co/In_2O_3, as benchmark RWGS-CL materials, were prepared following procedures described in the literature[11,14] (experimental details are provided in the ESI†).

X-ray diffraction (XRD) patterns of the samples were collected using an Ultima IV X-ray diffractometer (Rigaku) with Cu Kα radiation (λ = 1.54056 Å). The XRD patterns were obtained in the range 2θ = 20°–80° in steps of 0.01° at room temperature. In situ synchrotron X-ray diffraction (SXRD) patterns of the samples were obtained using a Debye–Scherrer camera with a two-dimensional detector (PILATUS 100 K) installed in the BL5S2 beamline at the Aichi Synchrotron Radiation Center. The quartz glass capillaries (0.3 mm o.d.) filled with the samples were irradiated with X-rays at a wavelength of λ = 0.689826 Å. The atmosphere in the capillaries was either air or 100% H_2. Both patterns were obtained at either room temperature or 500 °C. The collected XRD and *in situ* SXRD patterns were analyzed using the Le Bail method implemented in JANA2006.[24] Diffuse reflectance infrared Fourier transform (DRIFT) spectra of samples were recorded at 500 °C under a flow of 5% CO_2/N_2 (200 mL min⁻¹) using an iS50 spectrometer (Thermo Fisher). These samples (40 mg) were preheated at 500 °C for 30 min under a flow of 5% H_2/N_2 (200 mL min⁻¹). Thermogravimetric analysis (TGA) was conducted using a thermogravimeter analyzer (TGA-50, Shimadzu) connected to mass flow controllers. The temperature dependence of the TGA curves of the samples (20 mg) was recorded up to 800 °C at a ramp rate of 10 °C min⁻¹ under a flow of 5% H_2/N_2 (100 mL min⁻¹). The RWGS-CL performance of the samples (20 mg) was evaluated from the isothermal TGA curves recorded upon switching between a flow of 5% H_2/N_2 (100 mL min⁻¹) and 5% CO_2/N_2 (100 mL min⁻¹) every 30 min at 200–500 °C. The CO production rate was estimated from the weight loss during the initial 30 s under 5% H_2/N_2. The amount of CO produced was estimated from the total weight loss after 30 min under a 5% H_2/N_2 flow. CO production was also confirmed by additional experiments using a fixed bed reactor, in which the reaction gas can be analyzed by mass spectrometry (infiTOF, KANOMAX JAPAN) or Fourier-transform infrared (FT-IR) spectroscopy (Bex-100FT, Best-Sokki).

Results and discussion

All the XRD patterns of the synthesized samples (x = 0, 0.25, 0.5, 0.75, and 1) are characterized by a rhombohedral perovs-

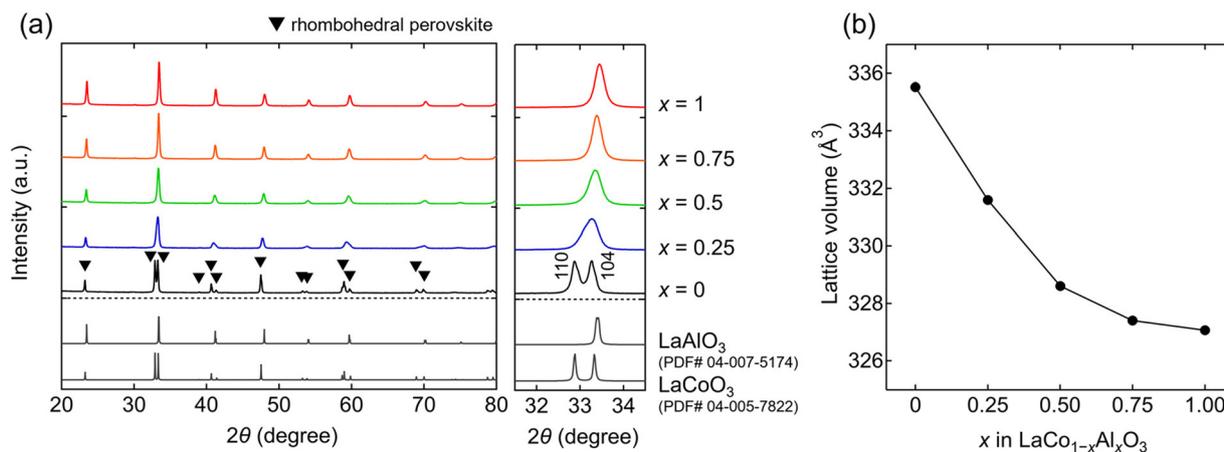**Fig. 2** (a) X-ray diffraction (XRD) patterns of LaCo$_{1-x}$Al$_x$O$_3$ (0 ≤ x ≤ 1). (b) Lattice volumes of LaCo$_{1-x}$Al$_x$O$_3$ as a function of Al content (x).

kite structure with a space group of $R\bar{3}c$ (Fig. 2a). No impurities were observed in any sample. The estimated lattice volumes of the end members were $V = 335.53(1)$ and $327.06(2)$ Å^3 for the $x = 0$ and 1 samples, respectively. These values agree with those reported for LaCoO$_3$ ($V = 335.6$ Å^3)[25] and LaAlO$_3$ ($V = 326.9$ Å^3),[26] respectively. The lattice volumes (Fig. 2b) of the rhombohedral perovskite phases decrease with increasing Al content (x), indicating the successful substitution of Al for Co in LaCo$_{1-x}$Al$_x$O$_3$. This is attributed to the smaller ionic radius of Al^{3+} (0.535 Å) compared to that of Co^{3+} (0.61 Å).[27] The 111 and 104 primary peaks at approximately $2\theta = 33°$, as shown in the $x = 0$ sample (LaCoO$_3$), overlapped into one peak with an increase in the Al content (Fig. 2a). This overlap is attributed to the reduction of octahedral tilting in the rhombohedral perovskite structure.[28]

The oxygen release behavior of LaCo$_{1-x}$Al$_x$O$_3$ is investigated using TGA, recorded upon heating to 800 °C under a flow of 5% H$_2$/N$_2$ (Fig. 3). The TGA curve of LaAlO$_3$ ($x = 1$) did not exhibit any weight loss upon heating to 800 °C, whereas all the
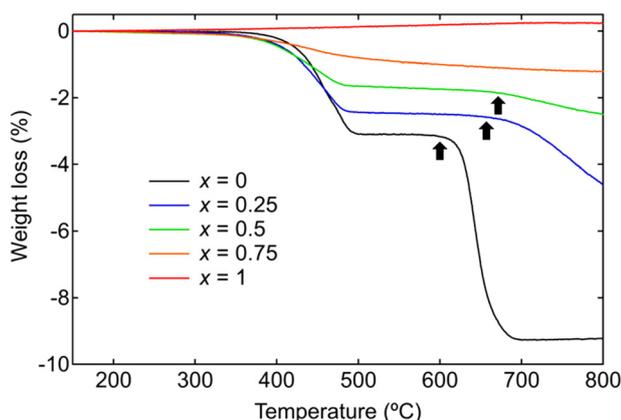
TGA curves of Co-containing LaCo$_{1-x}$Al$_x$O$_3$ ($x = 0$, 0.25, 0.5, 0.75) exhibited weight losses at 300–500 °C, indicating that these weight losses were attributed to the oxygen release associated with the reduction of Co^{3+}. The amount of weight loss up to 500 °C decreased with an increase in the Al content because of the decrease in the Co content. These weight losses correspond to the reduction of Co^{3+} to Co$^{2.04-2.11+}$. All XRD patterns of LaCo$_{1-x}$Al$_x$O$_3$ quenched at 500 °C in the TGA measurements are indexed by their original rhombohedral perovskite structure (space group: $R\bar{3}c$) without any separated phase (Fig. S1†). These observations suggest that Co-containing LaCo$_{1-x}$Al$_x$O$_3$ (Co^{3+}) transform into LaCo$_{1-x}$Al$_x$O$_{3-\delta}$ (Co^{2+}; $\delta = (1-x)/2$) following topotactic oxygen release from their crystal lattices.

The TGA curve of LaCoO$_3$ ($x = 0$) exhibited further weight loss in the range 600–700 °C. The weight loss up to 700 °C (9.3 wt%) was 3.0 times higher than that observed up to 500 °C (3.1 wt%), suggesting the sequential reduction of LaCoO$_3$ (Co^{3+}) into LaCoO$_{2.5}$ (Co^{2+}), followed by decomposition into Co (Co^0) and La$_2$O$_3$. The Co and La$_2$O$_3$ phases are shown in the XRD pattern of LaCoO$_3$ quenched at 800 °C in the TGA measurements (Fig. S2†), attributing the weight loss at 600–700 °C to phase decomposition. The phase decomposition temperature (black arrows in Fig. 3) increases with increasing Al content: 600, 660, and 670 °C for LaCoO$_3$ ($x = 0$), LaCo$_{0.75}$Al$_{0.25}$O$_3$ ($x = 0.25$), and LaCo$_{0.5}$Al$_{0.5}$O$_3$ ($x = 0.5$), respectively. LaCo$_{0.25}$Al$_{0.75}$O$_3$ ($x = 0.75$) and LaAlO$_3$ ($x = 1$) did not exhibit any significant weight loss in the range 500–800 °C. The XRD patterns of the samples quenched at 800 °C reveal that undergoes LaCo$_{0.75}$Al$_{0.25}$O$_3$ ($x = 0.25$) partial decomposition, while still maintaining the perovskite phase. LaCo$_{0.5}$Al$_{0.5}$O$_3$ ($x = 0.5$), LaCo$_{0.25}$Al$_{0.75}$O$_3$ ($x = 0.75$), and LaAlO$_3$ ($x = 1$) does not show any phase decomposition (Fig. S2†). These results show that Al substitution enhances the structural stability of perovskite LaCo$_{1-x}$Al$_x$O$_3$ in a reducing atmosphere.

In situ SXRD measurements were conducted to investigate the reasons for the enhanced structural stability. The SXRD patterns of LaCoO$_3$ ($x = 0$) and LaCo$_{0.5}$Al$_{0.5}$O$_3$ ($x = 0.5$) are

Fig. 3 Thermogravimetric analysis curves of LaCo$_{1-x}$Al$_x$O$_3$ (0 ≤ x ≤ 1) during heating in the flow of 5% H$_2$/N$_2$. Black arrows indicate the onset temperature of decomposition.

indexed to a rhombohedral perovskite structure (space group: $R\bar{3}c$) without any impurity phases at room temperature in air (Fig. 4). The estimated lattice volumes of $LaCoO_3$ and $LaCo_{0.5}Al_{0.5}O_3$ ($V = 335.80(3)$ and $329.25(4)$ Å^3, respectively, Fig. S3†) agreed with those estimated from the XRD patterns (Fig. 2). Heating these samples to 500 °C in air did not change their crystal structures. Peak shifts toward lower angles were observed for both samples, indicating an increase in the lattice volumes owing to thermal expansions.[29] The lattice volumes of $LaCoO_3$ and $LaCo_{0.5}Al_{0.5}O_3$ at 500 °C were $V = 347.80(6)$ and $336.62(5)$ Å^3, respectively (Fig. S3†), corresponding to thermal expansions of 3.6% and 2.2%, respectively, relative to those at room temperature. The SXRD pattern of $LaCoO_3$ obtained 5 min after switching the atmosphere from air to H_2 at 500 °C is characterized by an orthorhombic brownmillerite structure with a space group of $Pnma$ and a small amount of La_2O_3 (Fig. 4a). The brownmillerite structure was identical to the reported structure of $LaCoO_{2.5}$ ($La_2Co_2O_5$), which was produced by the reduction of $LaCoO_3$.[30] The brownmillerite phase observed in the SXRD pattern was identified as $LaCoO_{2.5}$. This determination was based on the estimated composition of $LaCoO_3$, which was found to be reduced at 500 °C in the TGA analysis ($LaCoO_{2.52}$), resulting in a composition similar to that of $LaCoO_{2.5}$. The peak intensities of the brownmillerite phase decreased 30 min after atmospheric switching, whereas those of La_2O_3 increased simultaneously.
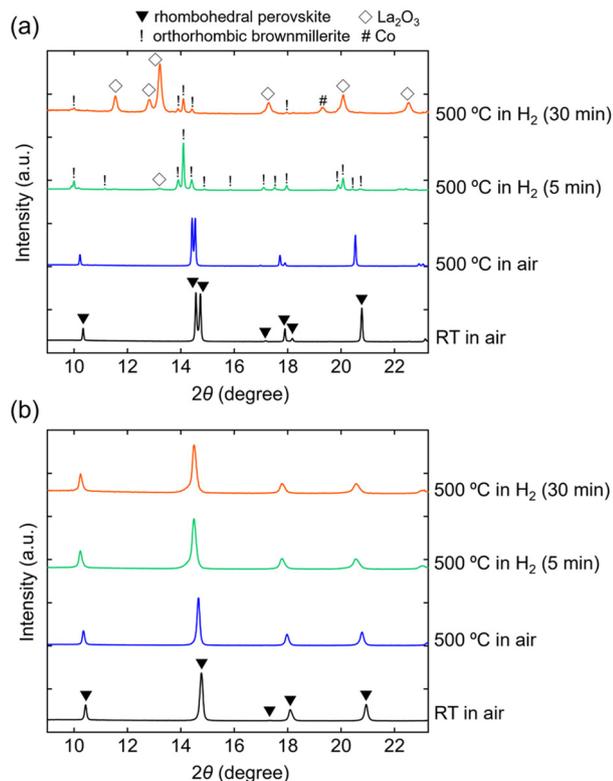
An additional Co metal phase was observed. These observations show that brownmillerite $LaCoO_{2.5}$, which is formed by the reduction of perovskite $LaCoO_3$, gradually decomposes into Co and La_2O_3 under a reducing atmosphere at 500 °C (Fig. 5). In contrast, the SXRD pattern of $LaCo_{0.5}Al_{0.5}O_3$ shows that the perovskite phase maintained its original rhombohedral perovskite structure 30 min after switching the atmosphere from air to H_2 at 500 °C (Fig. 4b). No phase decomposition was observed. Moreover, $LaCoO_3$ and $LaCo_{0.5}Al_{0.5}O_3$ exhibited an increase in the lattice volumes after switching the atmosphere from air to H_2 at 500 °C (Fig. S3†). This finding could be attributed to an increase in the ionic radius of Co from 0.61 Å (Co^{3+}) to 0.745 Å (Co^{2+}) owing to the reduction of $LaCoO_3$ and $LaCo_{0.5}Al_{0.5}O_3$. Therefore, *in situ* SXRD measurements suggest that the suppression of phase transition from the perovskite to the brownmillerite structure in a reducing atmosphere is responsible for the enhancement of the structural stability.

The effect of crystallographic differences on structural stability is often explained by the coordination number (CN) of redox species.[23,32] In perovskite $LaNi_{1-x}Al_xO_3$, suppression of the formation of Ni^{2+} with small CN (four-coordinated NiO_4) in a reducing atmosphere prevents further reduction to Ni^{0+}, leading to phase decomposition.[23] All Co atoms in the crystal lattice of $LaCoO_3$ and $LaCo_{0.5}Al_{0.5}O_3$ form CoO_6 octahedra (CN = 6) in an oxidizing atmosphere (Fig. 5). The brownmillerite $LaCoO_{2.5}$, observed for $LaCoO_3$ in a reducing atmosphere, has a vacancy-ordered structure comprising original CoO_6 octahedra and CoO_4 tetrahedra (CN = 4), where two O atoms are removed from the CoO_6 octahedra. Evidently, two oxygen atoms were removed from two neighboring octahedra in the perovskite structure; the formation of one tetrahedron that can form a vacancy-ordered structure is energetically more stable than the formation of two pentahedral (CN = 5).[33] In contrast, $LaCo_{0.5}Al_{0.5}O_3$ maintained its original rhombohedral perovskite structure in a reducing atmosphere, indicating that CoO_5

Fig. 4 In situ synchrotron XRD patterns of (a) $LaCoO_3$ and (b) $LaCo_{0.5}Al_{0.5}O_3$ collected at room temperature in air, 500 °C in air, and 500 °C in 100% H_2 (5 and 30 min).
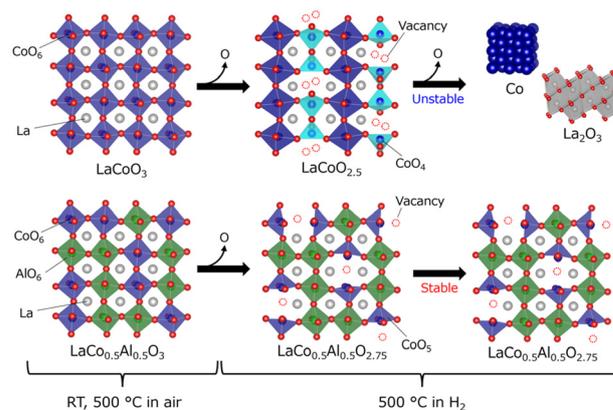
Fig. 5 Schematic of the structural changes in (a) $LaCoO_3$ and (b) $LaCo_{0.5}Al_{0.5}O_3$ at 500 °C. White, blue, green, and red spheres represent La, Co, Al, and O, respectively. The crystal structures were depicted by VESTA program.[31]

pentahedra rather than CoO_4 tetrahedra were predominantly formed by the reduction of $LaCo_{0.5}Al_{0.5}O_3$. This finding could be attributed to the random substitution of irreducible Al in $LaCo_{0.5}Al_{0.5}O_3$, which reduces the number of neighboring CoO_6 octahedra, preventing oxygen vacancy ordering resulting in the formation of CoO_4 tetrahedra. Suppression of the formation of CoO_4 tetrahedra with less CN enhanced the structural stability of $LaCo_{0.5}Al_{0.5}O_3$ in a reducing atmosphere.

The RWGS-CL performance of $LaCo_{1-x}Al_xO_3$ is evaluated from the weight change upon alternately switching the atmosphere between 5% H_2/N_2 and CO_2/N_2 every 30 min at an isothermal temperature of 500 °C (Fig. 6a). Co-containing $LaCo_{1-x}Al_xO_3$ (x = 0, 0.25, 0.5, and 0.75) exhibited weight losses in the initial 5% H_2/N_2 atmosphere (0–30 min) attributed to the oxygen release associated with Co^{3+} reduction. The amount of weight loss decreased with increasing Al content, indicating a decrease in the number of oxygen vacancies formed. The weights of the samples increased again when the atmosphere was switched to 5% CO_2/N_2 (30–60 min). The increase in weight was derived from oxygen intake associated with the oxidation of Co^{2+}, which resulted in the formation of CO through the reduction of CO_2. CO production was also confirmed by mass spectrometry (Fig. S4†) and FT-IR spectroscopy (Fig. S5†). Although these methods can quantify the CO production amount, they are not suitable for quantifying the CO production rate because of the effect of gas diffusion. Thus, CO production is often estimated from weight changes.[11,18] When the atmosphere was subsequently switched again to 5%

H_2/N_2 (60–90 min), the weight of $LaCo_{1-x}Al_xO_3$ (x = 0.25, 0.5, and 0.75) decreased to the same weight as that in the initial 5% H_2/N_2 atmosphere (0–30 min), whereas the weight of $LaCoO_3$ (x = 0) decreased more than that in the initial 5% H_2/N_2 atmosphere (0–30 min). The RWGS-CL profiles normalized by the fraction of reduced Co^{3+} ($[Co^{2+}]/([Co^{2+}] + [Co^{3+}])$) show that the fraction of $LaCo_{1-x}Al_xO_3$ (x = 0.25, 0.5, and 0.75) becomes constant at approximately 100% in 5% H_2/N_2, whereas that of $LaCoO_3$ exceeds 100% (Fig. S6†). This finding suggests that Co^{3+} in $LaCo_{1-x}Al_xO_3$ (x = 0.25, 0.5, and 0.75) is stabilized by Co^{2+} in a reducing atmosphere, whereas Co^{3+} in $LaCoO_3$ is not stabilized by Co^{2+} and is further reduced. The XRD patterns of samples after the RWGS-CL reaction (Fig. S7†) reveal that only $LaCoO_3$ contained La_2O_3 in addition to its original perovskite phase, indicating that the reduction of Co^{2+} is accompanied by a phase separation, which is consistent with the fact that $LaCoO_3$ gradually decomposes into Co and La_2O_3 in a reducing atmosphere, as revealed by the *in situ* SXRD experiment (Fig. 5). Therefore, the RWGS-CL reaction of $LaCo_{1-x}Al_xO_3$ (x = 0.25, 0.5, and 0.75) containing Co and Al corresponds to the following topotactic redox reactions:

$$LaCo_{1-x}Al_xO_3 + \delta H_2 \rightarrow LaCo_{1-x}Al_xO_{3-\delta} + \delta H_2O \qquad (1)$$

$$LaCo_{1-x}Al_xO_{3-\delta} + \delta CO_2 \rightarrow LaCo_{1-x}Al_xO_3 + \delta CO \qquad (2)$$
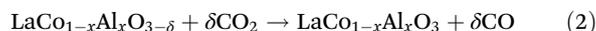
The CO production rate per unit mass (CO mol g^{-1} min^{-1}), which is estimated from the weight change rate in 5% CO_2/N_2 at 500 °C, is maximum at x = 0.5–0.75 for $LaCo_{1-x}Al_xO_3$ (Fig. 6b). For example, the CO production rate of $LaCo_{0.5}Al_{0.5}O_3$ (x = 0.5; 2.97×10^{-4} CO mol g^{-1} min^{-1}) was 4.1 times higher than that of $LaCoO_3$ (x = 0; 0.73×10^{-4} CO mol g^{-1} min^{-1}). The higher CO production rate per unit mass despite the lower Co content is derived from the fact that the CO production rate per Co atom (CO mol^{-1} min^{-1}) increased with increasing Al content (Fig. 6b: $0 \leq x \leq 0.75$). The DRIFT spectra of $LaCoO_3$ (x = 0) and $LaCo_{0.75}Al_{0.25}O_3$ (x = 0.25) in 5% CO_2/N_2 at 500 °C (Fig. S8†) exhibited only one absorption peak at approximately 2350 cm^{-1}, corresponding to the CO_2 gas phase,[34] whereas that of $LaCo_{0.5}Al_{0.5}O_3$ (x = 0.5) exhibited additional broad peaks at 1252 and 1529 cm^{-1} derived from carbonate (CO_3^{2-}).[35] However, the adsorption modes of carbonate could not be identified because of the broadness of the peaks. The oxygen atoms required for carbonate formation can come from $LaCo_{1-x}Al_xO_{3-\delta}$ itself or supplied to $LaCo_{1-x}Al_xO_{3-\delta}$ during the RWGS-CL reaction in eqn (2). $LaCo_{0.25}Al_{0.75}O_3$ (x = 0.75) had larger peaks at 1186 and 1685 cm^{-1}, originating from carbonates; however, $LaAlO_3$ (x = 1) did not exhibit any peaks associated with carbonates. The results of the DRIFT experiments suggest that the coexistence of a suitable amount of Al and Co ($0.5 \leq x \leq 0.75$) in $LaCo_{1-x}Al_xO_3$ increases the CO_2 adsorption sites. The increased number of CO_2 adsorption sites promotes CO_2 dissociation at an oxygen vacancy as an active site, which in turn enhances the CO production rate.

The CO production amount per unit mass (CO mol g^{-1}) at 500 °C is maximum at x = 0.5 ($LaCo_{0.5}Al_{0.5}O_3$; 4.67×10^{-4} CO
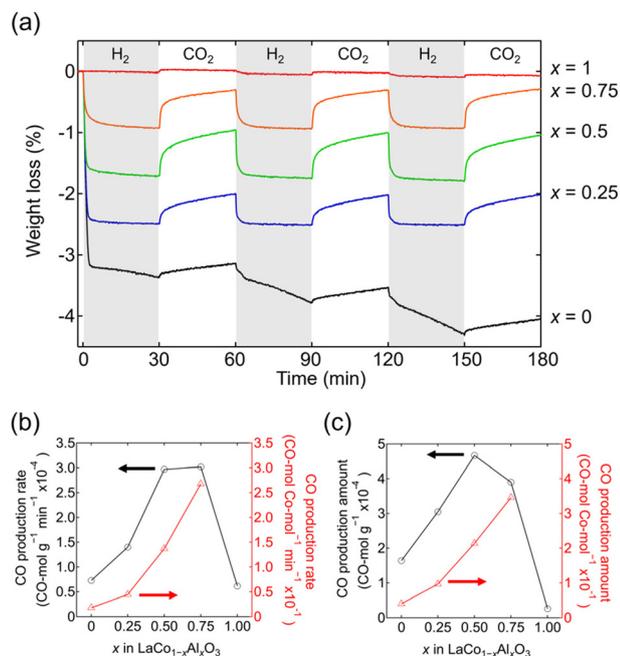

Fig. 6 (a) Isothermal RWGS-CL curves of $LaCo_{1-x}Al_xO_3$ ($0 \leq x \leq 1$) under flow of 5% H_2/N_2 and CO_2/N_2 at 500 °C. (b) CO production rate and (c) CO production amount of $LaCo_{1-x}Al_xO_3$ estimated from weight gains in 5% CO_2/N_2 at 500 °C.

mol g^{-1}) for LaCo$_{1-x}$Al$_x$O$_3$ (Fig. 6c). The amount of CO produced per Co atom (CO mol^{-1}) increased with an increase in the Al content ($0 \leq x \leq 0.75$) owing to the increase in the CO production rate. A trade-off between the increase in the CO production amount per Co atom and decrease in Co content would result in the maximum CO production amount per unit mass at $x = 0.5$. Additionally, the temperature dependence of the CO production amount per unit mass in the RWGS-CL reaction was investigated (Fig. S10†). LaCo$_{1-x}$Al$_x$O$_3$ (x = 0, 0.25, 0.5, 0.75, and 1) showed almost no CO production at 200 °C, whereas Co-containing LaCo$_{1-x}$Al$_x$O$_3$ (x = 0, 0.25, 0.5, and 0.75) produced CO at ≥300 °C. Interestingly, Al-substituted LaCo$_{1-x}$Al$_x$O$_3$ (x = 0.25, 0.5, and 0.75) produced more CO than LaCoO$_3$ (x = 0) at ≥400 °C, indicating the effect of the coexistence of Al and Co. Moreover, the amount of CO producing LaCo$_{0.5}$Al$_{0.5}$O$_3$ exhibits no degradation over 32 cycles of the RWGS-CL stability test at 500 °C (Fig. S9†), demonstrating that LaCo$_{0.5}$Al$_{0.5}$O$_3$ is usable as a practical RWGS-CL material.

The RWGS-CL performance of LaCo$_{0.5}$Al$_{0.5}$O$_3$ was then compared with those of perovskite La$_{0.6}$Ca$_{0.4}$Fe$_{0.4}$Mn$_{0.6}$O$_3$ (LCFMO)[14] and Co/In$_2$O$_3$,[11] which have been reported to exhibit high CO$_2$ conversion activity and stability. The order of the CO production rate at 500 °C is LCFMO > LaCo$_{0.5}$Al$_{0.5}$O$_3$ > Co/In$_2$O$_3$, which possibly reflects the order of the number of CO$_2$ adsorption sites or the activity of oxygen vacancies (Fig. S11a†). The CO production amount of Co/In$_2$O$_3$ (1.90×10^{-3} CO mol g^{-1}) is 4.0 and 3.3 times higher than that of LaCo$_{0.5}$Al$_{0.5}$O$_3$ (0.47×10^{-3} CO mol g^{-1}) and LCFMO (0.58×10^{-3} CO mol g^{-1}), respectively (Fig. S11b†). This finding is attributed to the fact that the theoretical maximum CO production amount estimated from the content of redox species in Co/In$_2$O$_3$ (In^{3+} ↔ In^0: 17.8 mmol g^{-1}) was 8.2 and 3.6 times higher than that of LaCo$_{0.5}$Al$_{0.5}$O$_3$ (Co^{3+} ↔ Co^{2+}: 2.18 mmol g^{-1}) and LCFMO (Fe^{3+} ↔ Fe^{2+} and Fe^{4+} ↔ Fe^{3+}: 4.93 mmol g^{-1}), respectively. Notably, the oxygen release rate, an indicator of regeneration rate of samples in H$_2$ atmosphere, of LaCo$_{0.5}$Al$_{0.5}$O$_3$ (6.02×10^{-4} O mol g^{-1} min^{-1}) is 6.4 and 4.7 times higher than that of LCFMO (0.94×10^{-4} O mol g^{-1} min^{-1}) and Co/In$_2$O$_3$ (1.27×10^{-4} O mol g^{-1} min^{-1}), respectively (Fig. S11c†). The oxygen release reaction in Co/In$_2$O$_3$ is associated with the formation of Co–In alloys from Co and In$_2$O$_3$,[11] whereas that in LaCo$_{0.5}$Al$_{0.5}$O$_3$ is accompanied by a topotactic reaction (eqn (1): from LaCo$_{0.5}$Al$_{0.5}$O$_3$ to LaCo$_{0.5}$Al$_{0.5}$O$_{2.75}$), which does not change the basic crystal structure. The relatively low energy required for oxygen release by the topotactic reaction may explain the higher oxygen release rate of LaCo$_{0.5}$Al$_{0.5}$O$_3$ than that of Co/In$_2$O$_3$. Moreover, the higher oxygen release rate of LaCo$_{0.5}$Al$_{0.5}$O$_3$ over that of LCFMO could be attributed to the fact that Co^{3+} is more readily reduced than Fe^{3+} and Mn^{4+}.[36] The RWGS-CL reaction system is expected to conduct reduction and oxidation reactions in parallel (Fig. 1); hence, RWGS-CL materials are required to exhibit high oxygen release and CO production rates. Therefore, LaCo$_{0.5}$Al$_{0.5}$O$_3$, with a high oxygen release rate in addition to a high CO production rate, is a suitable material for the RWGS-CL process.

Conclusions

Solid solutions of LaCo$_{1-x}$Al$_x$O$_3$ ($0 \leq x \leq 1$) with rhombohedral perovskites structure were synthesized using the polymerized complex method. The effect of Al substitution on their thermal stability in a reducing atmosphere and RWGS-CL performance was investigated. Al substitution suppressed the phase transition into a brownmillerite structure with ordered oxygen vacancies and enhanced the thermal stability in a reducing atmosphere. Hence, LaCo$_{0.5}$Al$_{0.5}$O$_3$ (x = 0.5) maintained the perovskite structure throughout a 32-cycle RWGS-CL stability test. Moreover, the CO production rate increased with Al substitution. The CO production rate of LaCo$_{0.5}$Al$_{0.5}$O$_3$ (2.97×10^{-4} CO mol g^{-1} min^{-1}) was 4.1 times higher than that of LaCoO$_3$ (0.73×10^{-4} CO mol g^{-1} min^{-1}). This activity enhancement may be derived from the CO$_2$ adsorption sites generated by the coexistence of Al and Co atoms. This study demonstrated that the substitution of Al, which was not involved in the redox reaction of RWGS-CL, exhibited the ability to enhance thermal stability in a reducing atmosphere and RWGS-CL performance. We believe that further compositional optimization of LaCo$_{1-x}$Al$_x$O$_3$ can lead to its practical application in the RWGS-CL process, thereby facilitating the utilization of CO$_2$.

Data availability

All data have been included in the manuscript and ESI.†

Author contributions

Yoshihiro Goto: data curation, investigation, visualization, writing – original draft. Kiyoshi Yamazaki: data curation, investigation, conceptualization, writing – review & editing. Masashi Kikugawa: conceptualization, methodology. Masakazu Aoki: conceptualization, project administration.

Conflicts of interest

There are no conflicts to declare.

Acknowledgements

References

1 IEACO$_2$ Emissions in 2022, https://www.iea.org/reports/co2-emissions-in-2022, (accessed May 2024).

2 S. Budinis, S. Krevor, N. M. Dowell, N. Brandon and A. Hawkes, *Energy Strat. Rev.*, 2018, **22**, 61.

3 J. Gibbins and H. Chalmers, *Energy Policy*, 2008, **36**, 4317.

4 Y. K. Kim, G. M. Kim and J. W. Lee, *J. Mater. Chem. A*, 2015, **3**, 10919.

5 Global CCS InstituteGlobal Status of CCS 2022, **https://www.globalccsinstitute.com/resources/global-status-of-ccs-2022/**, (accessed May 2024).

6 C. Breyer, M. Fasihi, C. Bajamundi and F. Creutzig, *Joule*, 2019, **3**, 2053.

7 N. von der Assen, P. Voll, M. Peters and A. Bardow, *Chem. Soc. Rev.*, 2014, **43**, 7982.

8 D. S. Mallapragada, N. R. Singh, V. Curteanu and R. Agrawal, *Ind. Eng. Chem. Res.*, 2013, **52**, 5136.

9 M. Gonzalez-Castano, B. Dorneanu and H. Arellano-Garcia, *React. Chem. Eng.*, 2021, **6**, 954.

10 H. Shi, V. R. Bhethanabotla and J. N. Kuhn, *J. Ind. Eng. Chem.*, 2023, **118**, 44.

11 J. Makiura, S. Kakihara, T. Higo, N. Ito, Y. Hirano and Y. Sekine, *Chem. Commun.*, 2022, **58**, 4837.

12 A. Thursfield, A. Murugan, R. Franca and I. S. Metcalfe, *Energy Environ. Sci.*, 2012, **5**, 7421.

13 M. Wenzel, L. Rihko-Strukmann and K. Sundmacher, *AIChE J.*, 2017, **63**, 15.

14 D. Maiti, B. J. Hare, Y. A. Daza, A. E. Ramos, J. N. Kuhn and V. R. Bhethanabotla, *Energy Environ. Sci.*, 2018, **11**, 648.

15 A. E. Ramos, D. Maiti, Y. A. Daza, J. N. Kuhn and V. R. Bhethanabotla, *Catal. Today*, 2019, **338**, 52.

16 H. Shi, V. R. Bhethanabotla and J. N. Kuhn, *J. Ind. Eng. Chem.*, 2023, **118**, 44.

17 H. S. Lim, Y. Kim, D. Kang, M. Lee, A. Jo and J. W. Lee, *ACS Catal.*, 2021, **11**, 12220.

18 K. Kang, S. Kakihara, T. Higo, H. Sampei, K. Saegusa and Y. Sekine, *Chem. Commun.*, 2023, **59**, 11061.

19 B. Wang, X. Wang, L. Lu, C. Zhou, Z. Xin, J. Wang, X. K. Ke, G. Sheng, S. Yan and Z. Zou, *ACS Catal.*, 2018, **8**, 516.

20 H. S. Lim, M. Lee, Y. Kim, D. Kang and J. W. Lee, *Int. J. Hydrogen Energy*, 2021, **46**, 15497.

21 L. Liu, D. D. Taylor, E. E. Rodriguez and M. R. Zachariah, *Chem. Commun.*, 2016, **52**, 10369.

22 A. A. Ansari, S. Adil, M. Alam, M. Assal, J. Labis and A. Alwarthan, *Sci. Rep.*, 2020, **10**, 15012.

23 Y. Goto, A. Morikawa, T. Tanabe and M. Iwasaki, *ACS Appl. Energy Mater.*, 2019, **2**, 3179.

24 V. Petříček, M. Dušek and L. Palatinus, *Z. Kristallogr. – Cryst. Mater.*, 2014, **229**, 345.

25 V. Narasimhan, V. H. Keer and D. K. Chakrabarty, *Phys. Status Solidi A*, 1985, **89**, 65.

26 S. Geller and V. B. Bala, *Acta Crystallogr.*, 1956, **9**, 1019.

27 R. D. Shannon, *Acta Crystallogr.*, 1976, **A32**, 751.

28 Q. N. Tran, F. Martinovic, M. Ceretti, S. Esposito, B. Bonelli, W. Paulus, F. Di Renzo, F. A. Deorsola, S. Bensaid and R. Pirone, *Appl. Catal., A*, 2020, **589**, 117304.

29 D. L. Anderson and D. G. Isaak, in *Mineral Physics and Crystallography: A Handbook of Physical Constants*, ed. T. J. Ahrens, American Geophysical Union, Washington DC, 1995, pp. 29–44.

30 O. H. Hansteen, H. Fjellvåg and B. C. Hauback, *J. Solid State Chem.*, 1998, **141**, 411.

31 K. Momma and F. Izumi, *J. Appl. Crystallogr.*, 2011, **44**, 1272.

32 A. Demizu, K. Beppu, S. Hosokawa, K. Kato, H. Asakura, K. Teramura and T. Tanaka, *J. Phys. Chem. C*, 2017, **121**, 19358.

33 S. Stølen, E. Bakken and C. E. Mohna, *Phys. Chem. Chem. Phys.*, 2006, **8**, 429.

34 F. Azzolina-Jury and F. Thibault-Starzyk, *Top. Catal.*, 2017, **60**, 1709.

35 N. H. Elsayed, D. Maiti, B. Joseph and J. N. Kurn, *Catal. Lett.*, 2018, **148**, 1003.

36 J. Daintith, *A Dictionary of Chemistry*, Oxford University Press, 2008.